Photocatalysis

DOI: 10.1002/anie.201410961

A Complex Perovskite-Type Oxynitride: The First Photocatalyst for Water Splitting Operable at up to 600 nm**

Chengsi Pan, Tsuyoshi Takata, Mamiko Nakabayashi, Takao Matsumoto, Naoya Shibata, Yuichi Ikuhara, and Kazunari Domen**

Abstract: *One of the simplest methods for splitting water into H_2 and O_2 with solar energy entails the use of a particulate-type semiconductor photocatalyst. To harness solar energy efficiently, a new water-splitting photocatalyst that is active over a wider range of the visible spectrum has been developed. In particular, a complex perovskite-type oxynitride, $LaMg_xTa_{1-x}O_{1+3x}N_{2-3x}$ ($x \geq 1/3$), can be employed for overall water splitting at wavelengths of up to 600 nm. Two effective strategies for overall water splitting were developed. The first entails the compositional fine-tuning of a photocatalyst to adjust the bandgap energy and position by forming a series of $LaMg_xTa_{1-x}O_{1+3x}N_{2-3x}$ solid solutions. The second method is based on the surface coating of the photocatalyst with a layer of amorphous oxyhydroxide to control the surface redox reactions. By combining these two strategies, the degradation of the photocatalyst and the reverse reaction could be prevented, resulting in successful overall water splitting.*

Direct water splitting into H_2 and O_2 on semiconductor photocatalysts is the most fundamental artificial photosynthetic reaction. A high-efficiency photocatalytic reaction using sunlight would offer an attractive means of producing clean and renewable energy. This would also be expected to be the most scalable and cost-effective route for large-scale renewable hydrogen production.[1] Although various kinds of photocatalysts for water splitting have been reported to date, most of these are only active under UV irradiation, and only a few have been demonstrated to operate under visible light,[2] up to a wavelength of approximately 500 nm.[3] Thus, the development of water-splitting photocatalysts with a narrower bandgap and a larger wavelength range is a significant target for efficient solar hydrogen production.

The typical metal oxynitrides with d^{10} electronic configuration, $(Ga_{1-x}Zn_x)(N_{1-x}O_x)$[4] and $(Zn_{1+x}Ge)(N_2O_x)$,[5] were found to be capable of direct water splitting into H_2 and O_2 under visible-light irradiation. However, they can utilize light with wavelengths below 480 nm, and only a limited portion of natural sunlight could be utilized. On the other hand, some d^0 transition-metal oxynitrides and nitrides containing Ti^{4+}, Nb^{5+}, or Ta^{5+} have bandgap energies of 1.8–2.1 eV, which corresponds to wavelengths of approximately 600 to 700 nm, and seem to have suitable bandgap positions for water splitting.[6] These transition-metal oxynitrides have been known to be potential water-splitting photocatalysts; however, all attempts to make use of such compounds have failed thus far, except for TaON,[7] with its bandgap energy of 2.4 eV ($\lambda = 510$ nm). The main difficulties are thought to be the lower energies available for H_2 and O_2 evolution and the lower stability of materials with narrower bandgap energies.

Herein, we introduce two effective strategies for the design of water-splitting photocatalysts with smaller bandgap energies by developing a newly designed Ta-based oxynitride photocatalyst with an absorption edge at approximately 600 nm. The first strategy entails the precise adjustment of the bandgap energy and position for water splitting by forming a series of solid solutions between two perovskite-type materials, namely the oxynitride $LaTaON_2$[8] and the complex oxide $LaMg_{2/3}Ta_{1/3}O_3$,[9] with comparable lattice constants. The general formula for the solid solution was taken to be $LaMg_xTa_{1-x}O_{1+3x}N_{2-3x}$ ($x = 0$–$2/3$) by mixing (1–

[*] Dr. C. Pan, Dr. T. Takata, Prof. K. Domen
Global Research Center for Environment and Energy Based on Nanomaterials Science (GREEN)
National Institute for Materials Science (NIMS)
1-1 Namiki, Tsukuba-city, Ibaraki, 305-0044 (Japan)
E-mail: TAKATA.Tsuyoshi@nims.go.jp
domen@chemsys.t.u-tokyo.ac.jp
M. Nakabayashi, Dr. T. Matsumoto, Prof. N. Shibata, Prof. Y. Ikuhara
Institute of Engineering Innovation
School of Engineering, The University of Tokyo
2-11-16, Yayoi, Bunkyo-ku, 113-8656 (Japan)
Prof. K. Domen
Department of Chemical System Engineering
School of Engineering, The University of Tokyo
7-3-1, Hongo, Bunkyo-ku, 113-8656 (Japan)
M. Nakabayashi, Prof. K. Domen
Japan Technological Research Association of Artificial Photosynthetic Chemical Process (ARPChem)
5-1-5 Kashiwanoha, Kashiwa-city, Ciba, 227-8589 (Japan)

[**] This work was supported in part by the "Development of Environmental Technology using Nanotechnology" program of the Ministry of Education, Culture, Sports, Science and Technology (MEXT; Japan), postdoctoral fellowships for foreign researchers from the Japan Society for the Promotion of Science, the Artificial Photosynthesis Project of the Ministry of Economy, Trade and Industry (METI), a Grant-in-Aid for Scientific Research (C; 24560953), and a Grant-in-Aid for Specially Promoted Research (23000009). Parts of this work were conducted at the Green Network of Excellence (GRENE) and supported by the "Nanotechnology Platform" (12024046), both sponsored by MEXT (Japan). We thank the Material Analysis Station at NIMS for performing the ICP measurement and O/N analysis.

Supporting information for this article is available on the WWW under http://dx.doi.org/10.1002/anie.201410961.

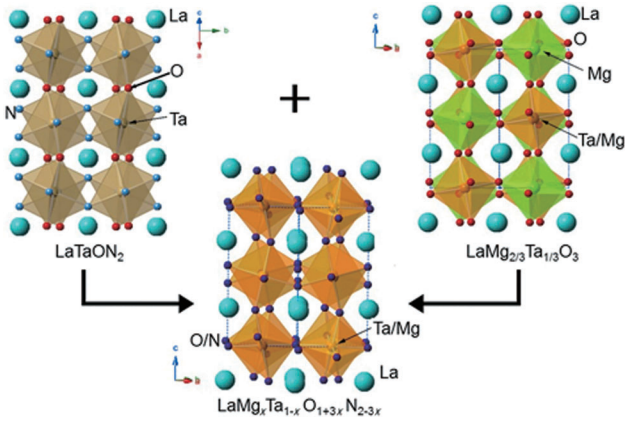

Scheme 1. Crystal structures of $LaMg_xTa_{1-x}O_{1+3x}N_{2-3x}$ ($x = 0$–2/3).

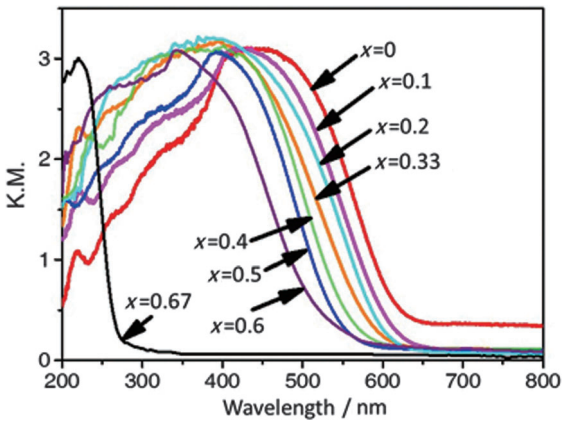

Figure 1. UV/Vis diffuse reflectance spectra of the $LaMg_xTa_{1-x}O_{1+3x}N_{2-3x}$ series. K.M. = Kubelka–Munk function.

3/2 x) $LaTaON_2$ and 3/2 x $LaMg_{2/3}Ta_{1/3}O_3$.[10] The crystal structures of the solid solutions are illustrated in Scheme 1. In a perovskite structure of this kind, Mg^{2+} (with an ionic radius of 72 pm) is known to selectively occupy Ta^{5+} (64 pm) sites, which concurrently causes substitution of O^{2-} (140 pm) for N^{3-} (150 pm) to maintain the overall charge balance as well as the original perovskite structure. Thus, Mg/Ta and O/N double substitution occurs. The synthesis and crystal structure analysis of the solid solutions have been reported previously,[10] but none of these materials have ever been examined as photocatalysts. The bandgap energy and position of the solid solution can be tuned by modifying the composition. This strategy has been examined for some transition-metal oxynitrides and has been confirmed to enhance H_2[11] or O_2[12] production in the presence of a sacrificial electron donor or acceptor, respectively. However, their ability to catalyze H_2 and O_2 production under such conditions is just a prerequisite for water splitting, and such works have not led to overall water splitting. Herein, this strategy was combined with a second one to achieve overall water splitting: The photocatalyst was subjected to a novel surface modification method to facilitate the surface reactions and stabilize the surface layer.

The $LaMg_xTa_{1-x}O_{1+3x}N_{2-3x}$ ($x = 0$–0.6) samples were synthesized by thermal ammonolysis of the corresponding oxide precursors, and the successful formation of the solid solutions was confirmed by X-ray diffraction (XRD) analysis (see the Supporting Information, Figure S1).

Next, the optical absorption properties of these materials were examined. As seen in the UV/Vis diffuse reflectance spectra in Figure 1, the wavelength of the absorption edge of $LaMg_xTa_{1-x}O_{1+3x}N_{2-3x}$ is blue-shifted monotonically from 640 to 525 nm when x is increased from 0 to 0.6. On the other hand, the absorption edge of $LaMg_{1/3}Ta_{2/3}O_3$ ($x = 2/3$) is located at 270 nm, at a far shorter wavelength than for the nitride samples. The bandgap energies of the solid solutions were estimated from the wavelengths of the absorption edges. The bandgap energy increased with increasing x, which may be mainly attributed to the shift in the level of the valence band maximum (VBM) as a result of the varied O and N content.[12a,b] Thermodynamically, this would be at least advantageous for O_2 production. The bandgap energy and position of a photocatalyst are thus tunable by forming a solid solution. The bandgap energies of $LaTaON_2$, $LaMg_{1/3}Ta_{2/3}O_2N$, and $LaMg_{2/3}Ta_{1/3}O_3$ were estimated to be 1.93, 2.08, and 4.59 eV, respectively, which are typical values for these materials.

The photocatalytic ability of this series of solid solutions ($x = 0$–0.6) for water splitting was examined. On all photocatalysts, a Rh/Cr mixed oxide [Rh (0.5 wt%) and Cr (0.5 wt%)], to be denoted by $RhCrO_y$, was loaded as a H_2 evolution cocatalyst.[13] First attempts at water splitting under light irradiation ($\lambda \geq 300$ nm) were carried out (Figure S2) and indicate that the solid solution with $x = 1/3$ was the most suitable one in this series for the water-splitting reaction.

To study the photocatalytic reaction on the sample with $x = 1/3$ in more detail, it was subjected to photoirradiation for prolonged periods of time (24 h × 2; Figure 2 a). N_2 evolution continued during the photoirradiation, which suggests that some holes (h^+) reacted with nitrogen species in the surface region. On the other hand, the amount of gaseous O_2 increased and then decreased during each irradiation period while the amount of gaseous H_2 continued to increase. This result suggests that the O_2 reduction reaction (ORR)

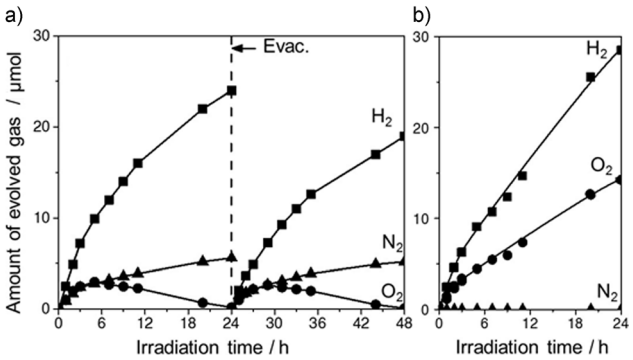

Figure 2. Gas evolution during water splitting on the catalysts $RhCrO_y$/$LaMg_{1/3}Ta_{2/3}O_2N$ (a) and $TiOXH/RhCrO_y/LaMg_{1/3}Ta_{2/3}O_2N$ (b). Reaction conditions: Catalyst (0.2 g), reaction solution: pure water (250 mL), Xe lamp (300 W); a side-irradiation-type reaction vessel made of Pyrex was used.

proceeded in competition with H_2O splitting, and the former reaction became dominant in the latter part of each reaction period. $RhCrO_y$ is known to act as a cocatalyst only for H^+ reduction, forming H_2 without promoting the ORR, that is, the reverse reaction of water splitting.[13] Therefore, the above result suggests that the ORR could proceed on the surface of $LaMg_{1/3}Ta_{2/3}O_2N$, and the accumulated h^+ continued to oxidize nitrogen species to form N_2.

Under this assumption, to prevent the ORR on the surface of $LaMg_{1/3}Ta_{2/3}O_2N$ and to suppress N_2 evolution, we attempted to coat the photocatalyst surface with a layer of an amorphous oxyhydroxide. We previously reported that the amorphous chromium oxyhydroxide $CrO_{1.5-m}(OH)_{2m}{\cdot}x\,H_2O$, a core/shell-type cocatalyst layer, worked as a selective permeation layer to facilitate water splitting and effectively prevent the ORR.[14] However, an attempt to coat the whole surface of the present photocatalyst with a $CrO_{1.5-m}(OH)_{2m}{\cdot}x\,H_2O$ overlayer by photodeposition of CrO_4^{2-} ions failed because the Cr^{III} oxyhydroxide was likely to be deposited only on the cocatalyst surface.[14a] We then attempted to deposit other amorphous materials as a coating layer to prevent the ORR and stabilize the photocatalyst surface.

Silica, titania, and their mixtures have been studied as coating layers. These materials are likely to be amorphous oxyhydroxides, generally formulated as $MO_{2-m}(OH)_{2m}{\cdot}x\,H_2O$ (M = Si, Ti). However, hereafter, they will be denoted by SiOXH and TiOXH. SiOXH deposition was performed by hydrolysis of tetraethyl orthosilicate (TEOS). For the deposition of TiOXH, a new modification method was devised, namely, photodeposition from a water-soluble Ti peroxide complex.[15] Peroxide complexes have an unusual valence state of O^{-I} in the peroxo ligand. This O^{-I} species can be easily reduced or oxidized to a more common valence state of O^{-II} or O^0, respectively. As the Ti peroxide complex is expected to be easily reduced or oxidized by photoexcited electrons or holes, photoirradiation of the photocatalyst in an aqueous solution containing the Ti peroxide complex would lead to decomposition of the peroxide complex to form a thin amorphous oxyhydroxide coating layer. Such an amorphous layer could indeed be formed as explained below.

The results for water splitting on TiOXH-coated $RhCrO_y$/$LaMg_{1/3}Ta_{2/3}O_2N$ are shown in Figure 2b. Details of the TiOXH photodeposition process are discussed in Figure S3. The photodeposition of TiOXH effectively prevented N_2 evolution and led to the simultaneous evolution of H_2 and O_2 with a ratio of nearly 2:1. A similar pretreatment in an aqueous H_2O_2 solution without any Ti source was also tested (Figure S4). Without TiOXH deposition, the water splitting reaction did not proceed efficiently. This result clearly indicates that the deposition of the TiOXH layer, rather than the treatment with H_2O_2, was essential for the observed overall water splitting. Heating of the TiOXH-deposited sample to form crystalline TiO_2 suppressed the photocatalytic activity (see Figure S5). On the other hand, with a SiOXH-coated $RhCrO_y$/$LaMg_{1/3}Ta_{2/3}O_2N$ catalyst, H_2 and O_2 evolution was observed, but significant N_2 evolution still occurred (Figure S6). Overall water splitting was achieved on the TiOXH-coated sample at this stage. The photocatalytic activities of the $LaMg_xTa_{1-x}O_{1+3x}N_{2-3x}$ series after TiOXH photodeposition are shown in Figure S7.

A double coating of SiOXH and TiOXH was also examined. The photodeposition of TiOXH on a SiOXH-coated sample enhanced the photocatalytic activity compared to the deposition of TiO_2 alone. The time courses of the water splitting reactions are shown in Figure 3. H_2 and O_2 evolution continued steadily for 22 hours with an intermediate evacuation of the gas phase. For irradiation with both $\lambda \geq 300$ nm and $\lambda \geq 420$ nm, stoichiometric H_2 and O_2 evolution proceeded at a constant rate, indicating that the ORR and N_2 evolution were successfully prevented. A double coating with TiOXH and SiOXH in the opposite order failed to suppress N_2 evolution (Figure S8). The dependence of the water-splitting activity on the cutoff wavelength of the incident light is illustrated in Figure S9. The onset wavelength agreed well with the absorption edge at 600 nm, which confirmed that bandgap excitation of $LaMg_{1/3}Ta_{2/3}O_2N$, not that of TiOXH, was responsible for water splitting.

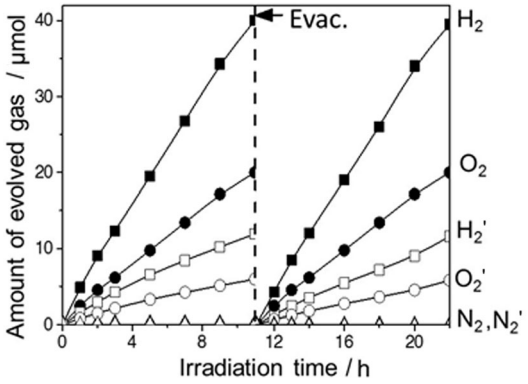

Figure 3. Gas evolution during water splitting on TiOXH/SiOXH/$RhCrO_y$/$LaMg_{1/3}Ta_{2/3}O_2N$ under UV/Vis irradiation ($\lambda \geq 300$ nm; filled symbols) and visible-light irradiation alone ($\lambda \geq 420$ nm; open symbols). Reaction conditions: Catalyst (0.2 g), reaction solution: pure water (250 mL), Xe lamp (300 W); a side-irradiation-type reaction vessel made of Pyrex was used.

The particle size of $LaMg_{1/3}Ta_{2/3}O_2N$ was 50–100 nm (Figure S10). The structure of the TiOXH/SiOXH-deposited sample was studied by scanning transmission electron microscopy (STEM) and energy dispersive X-ray spectroscopy (EDS). STEM-EDS elemental mapping of the TiOXH/SiOXH-deposited sample confirmed that the Si and Ti components were broadly dispersed over the whole surface of the photocatalyst particle, creating a core/shell-structured photocatalyst (Figure 4). High-resolution STEM images (Figure S11a) revealed an oxyhydroxide layer with a thickness of tens of nanometers on the surface of a photocatalyst particle. No lattice fringes were observed on the surface layer, indicating that the layer was amorphous. Furthermore, no crystalline TiO_2 phases were detected by XRD even when a substantial amount (20 wt%) of TiOXH had been deposited (Figure S11b).

Structural analysis revealed that both the H_2 and O_2 evolution sites were coated with a layer. In a structure of

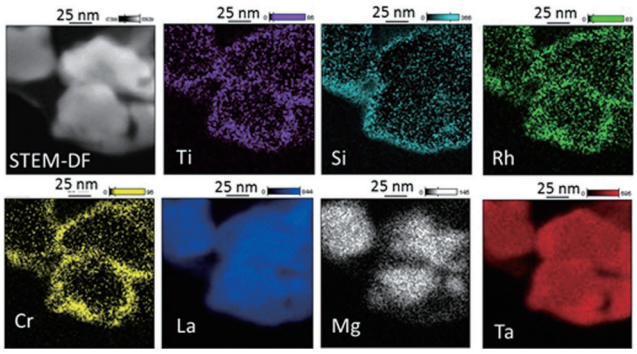

Figure 4. STEM-EDS elemental maps of TiOXH/SiOXH/$RhCrO_y$/$LaMg_{1/3}Ta_{2/3}O_2N$.

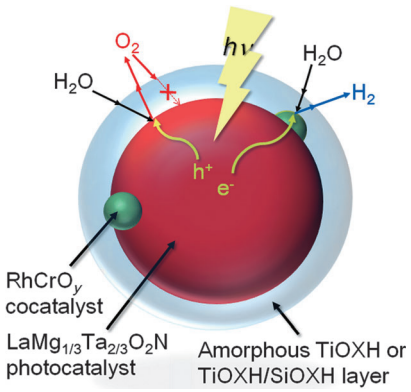

Figure 5. Reaction mechanism for water splitting on a surface-coated photocatalyst.

this kind, the reactant H_2O molecules could be supplied to the reaction sites on the surface of $RhCrO_y/LaMg_{1/3}Ta_{2/3}O_2N$ through the hydrated layer, and the H_2 and O_2 molecules produced could be released into the outer phase after permeating through the amorphous oxyhydroxide layer. The permeation of reactant and product molecules was likely enabled by the lattice flexibility in the amorphous layer. However, reverse diffusion of the released O_2 into the coating could be slowed or prevented, which suppressed the ORR on the photocatalyst. O_2 is generated by water oxidation at the interface between photocatalyst and coating. In this case, once O_2 molecules have been generated, they are temporarily confined in the narrow space; thereby, the partial pressure of O_2 in this space becomes higher than that in the ambient atmosphere, which may enable the one-way permeation of O_2 molecules. The TiOXH/SiOXH double coating likely acts by adjusting the density of the coating layer as well as the permeability of the reactants and products to achieve water splitting.

Coating the water oxidation site with an amorphous oxyhydroxide layer clearly suppressed N_2 evolution. One plausible explanation for this effect is that the prompt h^+ injection into oxygen species in the amorphous layer, that is, OH groups or hydrated water, prevented the excessive accumulation of h^+ in the nitrogen species on the photocatalyst surface. Thus, the water oxidation reaction could proceed at the interface between the oxynitride and the amorphous oxyhydroxide or in the amorphous oxyhydroxide layer. The reaction mechanism for water splitting on the surface-coated photocatalyst is summarized in Figure 5.

In summary, direct water splitting with visible light up to 600 nm was achieved for the first time by using a suitably modified $LaMg_xTa_{1-x}O_{1+3x}N_{2-3x}$ ($x \geq 1/3$) catalyst. Two effective approaches, compositional fine-tuning and surface coating, were developed. The quantum efficiency of overall water splitting is still low (ca. 0.03% at 440 ± 30 nm), and studies aimed at enhancing this efficiency are currently ongoing. The strategies used to develop this new photocatalyst are expected to be applicable to a wide range of materials and enable the fabrication of more efficient photocatalytic systems. Therefore, the development of our new photocatalyst system is encouraging and expected to be an important milestone for solar hydrogen production.

Experimental Section

Preparation of the photocatalyst: $LaMg_xTa_{1-x}O_{1+3x}N_{2-3x}$ was prepared by thermal ammonolysis of the corresponding oxide precursors. The oxide precursors were prepared by a citric acid method.[16] Then, the photocatalyst was loaded with a Rh/Cr mixed-oxide cocatalyst,[13] $RhCrO_y$, by an impregnation method. $RhCrO_y/LaMg_xTa_{1-x}O_{1+3x}N_{2-3x}$ was coated with SiOXH by hydrolysis of tetraethyl orthosilicate. TiOXH was deposited on $RhCrO_y/LaMg_xTa_{1-x}O_{1+3x}N_{2-3x}$ or SiOXH/$RhCrO_y/LaMg_xTa_{1-x}O_{1+3x}N_{2-3x}$ from an aqueous Ti peroxide solution by photodeposition. For further details of the photocatalyst preparation, see the Supporting Information.

Photocatalytic reaction: Reactions were carried out in a Pyrex side-irradiation-type reaction vessel connected to a closed gas circulation system made of Pyrex. An aqueous solution (250 mL) containing 0.2 g of the photocatalyst was used. Prior to the reaction, the solution was thoroughly evacuated to remove all air and then irradiated with a Xe lamp (300 W) with or without a cutoff filter for UV or visible-light irradiation. A flow of cooling water was used to maintain the reactant solution at room temperature. The evolved gases were analyzed by gas chromatography (thermal conductivity detector, molecular sieve (5 A) column, Ar carrier).

Characterization: The as-prepared samples were characterized by X-ray powder diffraction (XRD, Cu Kα radiation), field-emission scanning electron microscopy (FE-SEM), spherical-aberration-corrected field-emission scanning transmission electron microscopy (Cs-corrected FE-STEM), FE-STEM in combination with energy-dispersive X-ray spectroscopy (EDS), and UV/Vis diffuse reflectance spectroscopy (DRS).

Received: November 12, 2014
Published online: January 21, 2015

Keywords: coatings · oxynitrides · perovskite phases · photocatalysis · water splitting

[1] a) B. A. Pinaud, J. D. Benck, L. C. Seitz, A. J. Forman, Z. Chen, T. G. Deutsch, B. D. James, K. N. Baum, G. N. Baum, S. Ardo, H. Wang, E. Miller, T. F. Jaramillo, *Energy Environ. Sci.* **2013**, *6*, 1983 – 2002; b) U. Diebold, *Nat. Chem.* **2011**, *3*, 271 – 272.
[2] A. Kudo, Y. Miseki, *Chem. Soc. Rev.* **2009**, *38*, 253 – 278.
[3] a) R. Asai, H. Nemoto, Q. Jia, K. Saito, A. Iwase, A. Kudo, *Chem. Commun.* **2014**, *50*, 2543 – 2546; b) T. Hisatomi, J. Kubota, K. Domen, *Chem. Soc. Rev.* **2014**, *43*, 7520 – 7535.
[4] K. Maeda, K. Teramura, D. Lu, T. Takata, N. Saito, Y. Inoue, K. Domen, *Nature* **2006**, *440*, 295.

[5] Y. Lee, H. Terashima, Y. Shimodaira, K. Teramura, M. Hara, H. Kobayashi, K. Domen, M. Yashima, *J. Phys. Chem. C* **2007**, *111*, 1042 – 1048.
[6] K. Maeda, K. Domen, *J. Phys. Chem. Lett.* **2010**, *1*, 2655 – 2661.
[7] K. Maeda, D. Lu, K. Domen, *Chem. Eur. J.* **2013**, *19*, 4986 – 4991.
[8] E. Günther, R. Hagenmayer, M. Jansen, *Z. Anorg. Allg. Chem.* **2000**, *626*, 1519 – 1525.
[9] Y. Kim, P. Woodward, *J. Solid State Chem.* **2007**, *180*, 2798 – 2807.
[10] Y. Kim, P. Woodward, *J. Solid State Chem.* **2007**, *180*, 3224 – 3233.
[11] a) K. Maeda, K. Domen, *Angew. Chem. Int. Ed.* **2012**, *51*, 9865 – 9869; *Angew. Chem.* **2012**, *124*, 10003 – 10007; b) K. Maeda, H. Terashima, K. Kase, K. Domen, *Appl. Catal. A* **2009**, *357*, 206 – 212; c) P. Wu, J. Shi, Z. Zhou, W. Tang, L. Guo, *Int. J. Hydrogen Energy* **2012**, *37*, 13704 – 13710.
[12] a) K. Ueda, H. Kato, M. Kobayashi, M. Hara, M. Kakihana, *J. Mater. Chem. A* **2013**, *1*, 3667 – 3674; b) W. Luo, Z. Li, X. Jiang, T. Yu, L. Liu, X. Chen, J. Ye, Z. Zou, *Phys. Chem. Chem. Phys.* **2008**, *10*, 6717 – 6723; c) K. Maeda, D. Lu, K. Domen, *Angew. Chem. Int. Ed.* **2013**, *52*, 6488 – 6491; *Angew. Chem.* **2013**, *125*, 6616 – 6619.
[13] K. Maeda, K. Teramura, H. Masuda, T. Takata, N. Saito, Y. Inoue, K. Domen, *J. Phys. Chem. B* **2006**, *110*, 13107 – 13112.
[14] a) K. Maeda, K. Teramura, D. Lu, N. Saito, Y. Inoue, K. Domen, *Angew. Chem. Int. Ed.* **2006**, *45*, 7806 – 7809; *Angew. Chem.* **2006**, *118*, 7970 – 7973; b) M. Yoshida, K. Takanabe, K. Maeda, A. Ishikawa, J. Kubota, Y. Sakata, Y. Ikezawa, K. Domen, *J. Phys. Chem. C* **2009**, *113*, 10151 – 10157.
[15] J. Mühlebach, K. Müller, G. Schwarzenbach, *Inorg. Chem.* **1970**, *9*, 2381 – 2390.
[16] C. Marcilly, P. Courty, B. Delmon, *J. Am. Ceram. Soc.* **1970**, *53*, 56 – 57.

